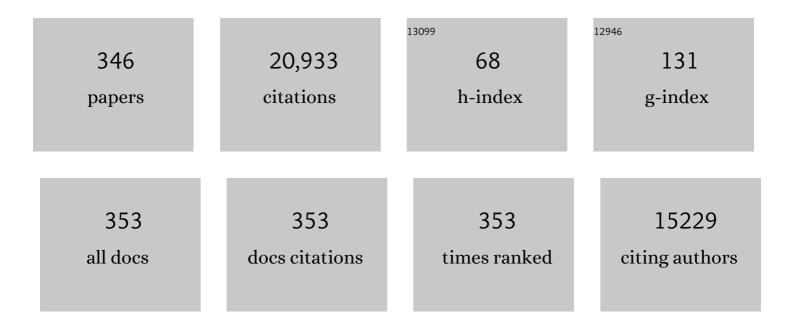
Scott B Reeder

List of Publications by Year in descending order

Source: https://exaly.com/author-pdf/9445281/publications.pdf Version: 2024-02-01



#	Article	IF	CITATIONS
1	Measurement of signalâ€toâ€noise ratios in MR images: Influence of multichannel coils, parallel imaging, and reconstruction filters. Journal of Magnetic Resonance Imaging, 2007, 26, 375-385.	3.4	809
2	Iterative decomposition of water and fat with echo asymmetry and least-squares estimation (IDEAL): Application with fast spin-echo imaging. Magnetic Resonance in Medicine, 2005, 54, 636-644.	3.0	615
3	Quantitative assessment of liver fat with magnetic resonance imaging and spectroscopy. Journal of Magnetic Resonance Imaging, 2011, 34, 729-749.	3.4	613
4	Gadolinium deposition in the brain: summary of evidence and recommendations. Lancet Neurology, The, 2017, 16, 564-570.	10.2	600
5	Multiecho waterâ€fat separation and simultaneous <i>R</i> estimation with multifrequency fat spectrum modeling. Magnetic Resonance in Medicine, 2008, 60, 1122-1134.	3.0	590
6	Tagged MR imaging in a deforming phantom: photographic validation Radiology, 1994, 190, 765-769.	7.3	459
7	Magnitude and Time Course of Microvascular Obstruction and Tissue Injury After Acute Myocardial Infarction. Circulation, 1998, 98, 1006-1014.	1.6	453
8	Multicoil Dixon chemical species separation with an iterative least-squares estimation method. Magnetic Resonance in Medicine, 2004, 51, 35-45.	3.0	449
9	Fat quantification with IDEAL gradient echo imaging: Correction of bias from <i>T</i> ₁ and noise. Magnetic Resonance in Medicine, 2007, 58, 354-364.	3.0	418
10	Proton density fatâ€fraction: A standardized mrâ€based biomarker of tissue fat concentration. Journal of Magnetic Resonance Imaging, 2012, 36, 1011-1014.	3.4	385
11	Multiecho reconstruction for simultaneous waterâ€fat decomposition and T2* estimation. Journal of Magnetic Resonance Imaging, 2007, 26, 1153-1161.	3.4	366
12	Quantitative assessment of liver fat with magnetic resonance imaging and spectroscopy. Journal of Magnetic Resonance Imaging, 2011, 34, 729-749.	3.4	359
13	Quantification of Hepatic Steatosis with T1-independent, T2*-corrected MR Imaging with Spectral Modeling of Fat: Blinded Comparison with MR Spectroscopy. Radiology, 2011, 258, 767-775.	7.3	345
14	Water–fat separation with IDEAL gradient-echo imaging. Journal of Magnetic Resonance Imaging, 2007, 25, 644-652.	3.4	300
15	Noninvasive, Quantitative Assessment of Liver Fat by MRIâ€PDFF as an Endpoint in NASH Trials. Hepatology, 2018, 68, 763-772.	7.3	299
16	Fat and water magnetic resonance imaging. Journal of Magnetic Resonance Imaging, 2010, 31, 4-18.	3.4	291
17	Practical approaches to the evaluation of signal-to-noise ratio performance with parallel imaging: Application with cardiac imaging and a 32-channel cardiac coil. Magnetic Resonance in Medicine, 2005, 54, 748-754.	3.0	274
18	Quantification of Liver Fat with Magnetic Resonance Imaging. Magnetic Resonance Imaging Clinics of North America, 2010, 18, 337-357.	1.1	260

#	Article	IF	CITATIONS
19	Effects of refocusing flip angle modulation and view ordering in 3D fast spin echo. Magnetic Resonance in Medicine, 2008, 60, 640-649.	3.0	239
20	Linearity, Bias, and Precision of Hepatic Proton Density Fat Fraction Measurements by Using MR Imaging: A Meta-Analysis. Radiology, 2018, 286, 486-498.	7.3	225
21	Quantification of hepatic steatosis with MRI: The effects of accurate fat spectral modeling. Journal of Magnetic Resonance Imaging, 2009, 29, 1332-1339.	3.4	221
22	Quantification of liver iron with MRI: State of the art and remaining challenges. Journal of Magnetic Resonance Imaging, 2014, 40, 1003-1021.	3.4	208
23	Influence of multichannel combination, parallel imaging and other reconstruction techniques on MRI noise characteristics. Magnetic Resonance Imaging, 2008, 26, 754-762.	1.8	199
24	Field map estimation with a region growing scheme for iterative 3-point water-fat decomposition. Magnetic Resonance in Medicine, 2005, 54, 1032-1039.	3.0	195
25	Cramér-Rao bounds for three-point decomposition of water and fat. Magnetic Resonance in Medicine, 2005, 54, 625-635.	3.0	194
26	T ₁ independent, T ₂ * corrected MRI with accurate spectral modeling for quantification of fat: Validation in a fatâ€water‧PIO phantom. Journal of Magnetic Resonance Imaging, 2009, 30, 1215-1222.	3.4	191
27	In vivo measurement of T*2 and field inhomogeneity maps in the human heart at 1.5 T. Magnetic Resonance in Medicine, 1998, 39, 988-998.	3.0	183
28	T ₁ independent, T ₂ [*] corrected chemical shift based fat–water separation with multiâ€peak fat spectral modeling is an accurate and precise measure of hepatic steatosis. Journal of Magnetic Resonance Imaging, 2011, 33, 873-881.	3.4	183
29	Accuracy of Liver Fat Quantification With Advanced CT, MRI, and Ultrasound Techniques: Prospective Comparison With MR Spectroscopy. American Journal of Roentgenology, 2017, 208, 92-100.	2.2	180
30	Safety and technique of ferumoxytol administration for MRI. Magnetic Resonance in Medicine, 2016, 75, 2107-2111.	3.0	171
31	Magnetic Resonance Imaging Quantification of Liver Iron. Magnetic Resonance Imaging Clinics of North America, 2010, 18, 359-381.	1.1	170
32	Advanced MRI Methods for Assessment of Chronic Liver Disease. American Journal of Roentgenology, 2009, 193, 14-27.	2.2	169
33	Effect of Multipeak Spectral Modeling of Fat for Liver Iron and Fat Quantification: Correlation of Biopsy with MR Imaging Results. Radiology, 2012, 265, 133-142.	7.3	169
34	Combination of complexâ€based and magnitudeâ€based multiecho waterâ€fat separation for accurate quantification of fatâ€fraction. Magnetic Resonance in Medicine, 2011, 66, 199-206.	3.0	166
35	Evaluation for Myocarditis in Competitive Student Athletes Recovering From Coronavirus Disease 2019 With Cardiac Magnetic Resonance Imaging. JAMA Cardiology, 2021, 6, 945.	6.1	161
36	Repeatability of magnetic resonance elastography for quantification of hepatic stiffness. Journal of Magnetic Resonance Imaging, 2010, 31, 725-731.	3.4	145

#	Article	IF	CITATIONS
37	4D cardiovascular magnetic resonance velocity mapping of alterations of right heart flow patterns and main pulmonary artery hemodynamics in tetralogy of Fallot. Journal of Cardiovascular Magnetic Resonance, 2012, 14, 16.	3.3	129
38	Quantitative magnetic resonance imaging of hepatic steatosis: Validation in ex vivo human livers. Hepatology, 2015, 62, 1444-1455.	7.3	128
39	MR imaging of articular cartilage at 1.5T and 3.0T: Comparison of SPGR and SSFP sequences. Osteoarthritis and Cartilage, 2005, 13, 338-344.	1.3	124
40	Hepatobiliary MR imaging with gadoliniumâ€based contrast agents. Journal of Magnetic Resonance Imaging, 2012, 35, 492-511.	3.4	121
41	Multipeak fatâ€corrected complex R2* relaxometry: Theory, optimization, and clinical validation. Magnetic Resonance in Medicine, 2013, 70, 1319-1331.	3.0	115
42	Pancreatic Steatosis Demonstrated at MR Imaging in the General Population: Clinical Relevance. Radiology, 2015, 276, 129-136.	7.3	113
43	Fast ²³ Na Magnetic Resonance Imaging of Acute Reperfused Myocardial Infarction. Circulation, 1997, 95, 1877-1885.	1.6	109
44	Proton-density fat fraction and simultaneous R2* estimation as an MRI tool for assessment of osteoporosis. European Radiology, 2013, 23, 3432-3439.	4.5	106
45	Addressing phase errors in fatâ€water imaging using a mixed magnitude/complex fitting method. Magnetic Resonance in Medicine, 2012, 67, 638-644.	3.0	105
46	Dermal white adipose tissue: a new component of the thermogenic response. Journal of Lipid Research, 2015, 56, 2061-2069.	4.2	104
47	Diagnosis of Coronavirus Disease 2019 Pneumonia by Using Chest Radiography: Value of Artificial Intelligence. Radiology, 2021, 298, E88-E97.	7.3	102
48	Multisite, multivendor validation of the accuracy and reproducibility of proton-density fat-fraction quantification at 1.5T and 3T using a fat-water phantom. Magnetic Resonance in Medicine, 2017, 77, 1516-1524.	3.0	99
49	Quantitative susceptibility mapping in the abdomen as an imaging biomarker of hepatic iron overload. Magnetic Resonance in Medicine, 2015, 74, 673-683.	3.0	98
50	In vivo validation of 4D flow MRI for assessing the hemodynamics of portal hypertension. Journal of Magnetic Resonance Imaging, 2013, 37, 1100-1108.	3.4	93
51	Leastâ€squares chemical shift separation for ¹³ C metabolic imaging. Journal of Magnetic Resonance Imaging, 2007, 26, 1145-1152.	3.4	91
52	Prevalence of Fatty Liver Disease and Hepatic Iron Overload in a Northeastern German Population by Using Quantitative MR Imaging. Radiology, 2017, 284, 706-716.	7.3	91
53	Sonography in Primary Hyperparathyroidism. Journal of Ultrasound in Medicine, 2002, 21, 539-552.	1.7	90
54	Cardiac MRI of ischemic heart disease at 3T: Potential and challenges. European Journal of Radiology, 2008. 65. 15-28.	2.6	83

#	Article	IF	CITATIONS
55	Generalized <i>k</i> â€space decomposition with chemical shift correction for nonâ€cartesian waterâ€fat imaging. Magnetic Resonance in Medicine, 2008, 59, 1151-1164.	3.0	81
56	R mapping in the presence of macroscopic <i>B</i> _O field variations. Magnetic Resonance in Medicine, 2012, 68, 830-840.	3.0	80
57	The influence of prior hamstring injury on lengthening muscle tissue mechanics. Journal of Biomechanics, 2010, 43, 2254-2260.	2.1	79
58	Cardiovascular Magnetic Resonance for Patients With COVID-19. JACC: Cardiovascular Imaging, 2022, 15, 685-699.	5.3	79
59	Independent estimation of <i>T</i> * ₂ for water and fat for improved accuracy of fat quantification. Magnetic Resonance in Medicine, 2010, 63, 849-857.	3.0	78
60	Quantitative chemical shift-encoded MRI is an accurate method to quantify hepatic steatosis. Journal of Magnetic Resonance Imaging, 2014, 39, 1494-1501.	3.4	78
61	Value of MRI in medicine: More than just another test?. Journal of Magnetic Resonance Imaging, 2019, 49, e14-e25.	3.4	78
62	An Investigation of Transient Severe Motion Related to Gadoxetic Acid–enhanced MR Imaging. Radiology, 2016, 279, 93-102.	7.3	77
63	Quantification of Liver Fat Content with CT and MRI: State of the Art. Radiology, 2021, 301, 250-262.	7.3	77
64	Multi-echo segmented k-space imaging: An optimized hybrid sequence for ultrafast cardiac imaging. Magnetic Resonance in Medicine, 1999, 41, 375-385.	3.0	74
65	Rapid MR Imaging of Articular Cartilage with Steady-State Free Precession and Multipoint Fat-Water Separation. American Journal of Roentgenology, 2003, 180, 357-362.	2.2	74
66	Water–fat separation with bipolar multiecho sequences. Magnetic Resonance in Medicine, 2008, 60, 198-209.	3.0	73
67	Quantification of Liver Fat Content With Unenhanced MDCT: Phantom and Clinical Correlation With MRI Proton Density Fat Fraction. American Journal of Roentgenology, 2018, 211, W151-W157.	2.2	73
68	Quantification of Hepatic Steatosis With Dual-Energy Computed Tomography. Investigative Radiology, 2012, 47, 603-610.	6.2	72
69	Homodyne reconstruction and IDEAL water-fat decomposition. Magnetic Resonance in Medicine, 2005, 54, 586-593.	3.0	71
70	Cardiac CINE MR imaging with a 32-channel cardiac coil and parallel imaging: Impact of acceleration factors on image quality and volumetric accuracy. Journal of Magnetic Resonance Imaging, 2006, 23, 222-227.	3.4	71
71	Quantification of Hepatic Steatosis with 3-T MR Imaging: Validation in <i>ob/ob</i> Mice. Radiology, 2010, 254, 119-128.	7.3	71
72	Articular Cartilage of the Knee: Rapid Three-dimensional MR Imaging at 3.0 T with IDEAL Balanced Steady-State Free Precession—Initial Experience. Radiology, 2006, 240, 546-551.	7.3	70

#	Article	IF	CITATIONS
73	Body MRI Using IDEAL. American Journal of Roentgenology, 2008, 190, 1076-1084.	2.2	70
74	Characterization of hepatic adenoma and focal nodular hyperplasia with gadoxetic acid. Journal of Magnetic Resonance Imaging, 2012, 36, 686-696.	3.4	70
75	Quantitative Imaging Biomarkers of NAFLD. Digestive Diseases and Sciences, 2016, 61, 1337-1347.	2.3	70
76	Effects of water exchange on the measurement of myocardial perfusion using paramagnetic contrast agents. Magnetic Resonance in Medicine, 1999, 41, 334-342.	3.0	68
77	Natural History of Hepatic Steatosis: Observed Outcomes for Subsequent Liver and Cardiovascular Complications. American Journal of Roentgenology, 2014, 202, 752-758.	2.2	68
78	Standardized Approach for ROI-Based Measurements of Proton Density Fat Fraction and R2* in the Liver. American Journal of Roentgenology, 2017, 209, 592-603.	2.2	68
79	IDEAL Imaging of the Musculoskeletal System: Robust Water–Fat Separation for Uniform Fat Suppression, Marrow Evaluation, and Cartilage Imaging. American Journal of Roentgenology, 2007, 189, W284-W291.	2.2	67
80	Reproducibility of MRâ€based liver fat quantification across field strength: Sameâ€day comparison between 1.5T and 3T in obese subjects. Journal of Magnetic Resonance Imaging, 2015, 42, 811-817.	3.4	67
81	Time-Resolved Interventional Cardiac C-arm Cone-Beam CT: An Application of the PICCS Algorithm. IEEE Transactions on Medical Imaging, 2012, 31, 907-923.	8.9	66
82	Endovascular Abdominal Aortic Aneurysm Repair: Nonenhanced Volumetric CT for Follow-up. Radiology, 2009, 253, 253-262.	7.3	63
83	Phase and amplitude correction for multiâ€echo water–fat separation with bipolar acquisitions. Journal of Magnetic Resonance Imaging, 2010, 31, 1264-1271.	3.4	63
84	Noninvasive temperature mapping with MRI using chemical shift waterâ€fat separation. Magnetic Resonance in Medicine, 2010, 63, 1238-1246.	3.0	63
85	Presurgical Localization of the Artery of Adamkiewicz with Time-resolved 3.0-T MR Angiography. Radiology, 2010, 255, 873-881.	7.3	62
86	Cardiac CINE imaging with IDEAL water-fat separation and steady-state free precession. Journal of Magnetic Resonance Imaging, 2005, 22, 44-52.	3.4	61
87	Effectiveness of MR angiography for the primary diagnosis of acute pulmonary embolism: Clinical outcomes at 3 months and 1 year. Journal of Magnetic Resonance Imaging, 2013, 38, 914-925.	3.4	61
88	MRIâ€based quantitative susceptibility mapping (QSM) and R2* mapping of liver iron overload: Comparison with SQUIDâ€based biomagnetic liver susceptometry. Magnetic Resonance in Medicine, 2017, 78, 264-270.	3.0	61
89	Relaxivity of Ferumoxytol at 1.5 T and 3.0 T. Investigative Radiology, 2018, 53, 257-263.	6.2	61
90	ACR guidance document on MR safe practices: Updates and critical information 2019. Journal of Magnetic Resonance Imaging, 2020, 51, 331-338.	3.4	61

#	Article	IF	CITATIONS
91	Phase-Sensitive Inversion Recovery (PSIR) Single-Shot TrueFISP for Assessment of Myocardial Infarction at 3 Tesla. Investigative Radiology, 2006, 41, 148-153.	6.2	59
92	Blood oxygenation dependence oft1 andt2 in the isolated, perfused rabbit heart at 4.7t. Magnetic Resonance in Medicine, 1995, 34, 623-627.	3.0	58
93	Quantification and reduction of ghosting artifacts in interleaved echo-planar imaging. Magnetic Resonance in Medicine, 1997, 38, 429-439.	3.0	56
94	Noninvasive Assessment of Transstenotic Pressure Gradients in Porcine Renal Artery Stenoses by Using Vastly Undersampled Phase-Contrast MR Angiography. Radiology, 2011, 261, 266-273.	7.3	56
95	Presurgical Localization of Parathyroid Adenomas with Magnetic Resonance Imaging at 3.0 T: An Adjunct Method to Supplement Traditional Imaging. Annals of Surgical Oncology, 2012, 19, 981-989.	1.5	56
96	On the confounding effect of temperature on chemical shiftâ€encoded fat quantification. Magnetic Resonance in Medicine, 2014, 72, 464-470.	3.0	56
97	Referenceless interleaved echo-planar imaging. Magnetic Resonance in Medicine, 1999, 41, 87-94.	3.0	55
98	3.0-T Evaluation of Knee Cartilage by Using Three-Dimensional IDEAL GRASS Imaging: Comparison with Fast Spin-Echo Imaging. Radiology, 2010, 255, 117-127.	7.3	55
99	Optimized highâ€resolution contrastâ€enhanced hepatobiliary imaging at 3 tesla: A crossâ€over comparison of gadobenate dimeglumine and gadoxetic acid. Journal of Magnetic Resonance Imaging, 2011, 34, 585-594.	3.4	55
100	Effects of Inhaled Fluticasone on Upper Airway during Sleep and Wakefulness in Asthma: A Pilot Study. Journal of Clinical Sleep Medicine, 2014, 10, 183-193.	2.6	54
101	Proton density fat-fraction is an accurate biomarker of hepatic steatosis in adolescent girls and young women. European Radiology, 2015, 25, 2921-2930.	4.5	54
102	The effect of high performance gradients on fast gradient echo imaging. Magnetic Resonance in Medicine, 1994, 32, 612-621.	3.0	52
103	Sensitivity of chemical shiftâ€encoded fat quantification to calibration of fat MR spectrum. Magnetic Resonance in Medicine, 2016, 75, 845-851.	3.0	52
104	A magnetization-driven gradient echo pulse sequence for the study of myocardial perfusion. Magnetic Resonance in Medicine, 1995, 34, 276-282.	3.0	51
105	Renal Arteries: Isotropic, High-Spatial-Resolution, Unenhanced MR Angiography with Three-dimensional Radial Phase Contrast. Radiology, 2011, 258, 254-260.	7.3	51
106	High resolution navigated threeâ€dimensional T ₁ â€weighted hepatobiliary MRI using gadoxetic acid optimized for 1.5 tesla. Journal of Magnetic Resonance Imaging, 2012, 36, 890-899.	3.4	51
107	T1- and T2-weighted fast spin-echo imaging of the brachial plexus and cervical spine with IDEAL water–fat separation. Journal of Magnetic Resonance Imaging, 2006, 24, 825-832.	3.4	50
108	Fourâ€dimensional velocity mapping of the hepatic and splanchnic vasculature with radial sampling at 3 tesla: A feasibility study in portal hypertension. Journal of Magnetic Resonance Imaging, 2011, 34, 577-584.	3.4	50

#	Article	IF	CITATIONS
109	Advanced Cardiac MR Imaging of Ischemic Heart Disease. Radiographics, 2001, 21, 1047-1074.	3.3	49
110	Signal-to-noise ratio behavior of steady-state free precession. Magnetic Resonance in Medicine, 2004, 52, 123-130.	3.0	48
111	Impaired regulation of portal venous flow in response to a meal challenge as quantified by 4D flow MRI. Journal of Magnetic Resonance Imaging, 2015, 42, 1009-1017.	3.4	48
112	Myocarditis Associated with mRNA COVID-19 Vaccination. Radiology, 2021, 301, E409-E411.	7.3	48
113	Comparison of <i>R</i> ₂ * correction methods for accurate fat quantification in fatty liver. Journal of Magnetic Resonance Imaging, 2013, 37, 414-422.	3.4	47
114	Effects of postprandial state and mesenteric blood flow on the repeatability of MR elastography in asymptomatic subjects. Journal of Magnetic Resonance Imaging, 2011, 33, 239-244.	3.4	46
115	Hepatobiliary MR contrast agents in hypovascular hepatocellular carcinoma. Journal of Magnetic Resonance Imaging, 2015, 41, 251-265.	3.4	46
116	Intravenous Gadoxetate Disodium Administration Reduces Breath-holding Capacity in the Hepatic Arterial Phase: A Multi-Center Randomized Placebo-controlled Trial. Radiology, 2017, 282, 361-368.	7.3	46
117	How bariatric surgery affects liver volume and fat density in NAFLD patients. Surgical Endoscopy and Other Interventional Techniques, 2018, 32, 1675-1682.	2.4	46
118	Clinical Usefulness of Adding 3D Cartilage Imaging Sequences to a Routine Knee MR Protocol. American Journal of Roentgenology, 2011, 196, 159-167.	2.2	45
119	On the performance of <i>T</i> ₂ * correction methods for quantification of hepatic fat content. Magnetic Resonance in Medicine, 2012, 67, 389-404.	3.0	44
120	Quantification of Thoracic Blood Flow Using Volumetric Magnetic Resonance Imaging With Radial Velocity Encoding. Investigative Radiology, 2013, 48, 819-825.	6.2	44
121	Effect of flip angle on the accuracy and repeatability of hepatic proton density fat fraction estimation by complex dataâ€based, T1â€independent, T2*â€corrected, spectrumâ€modeled MRI. Journal of Magnetic Resonance Imaging, 2014, 39, 440-447.	3.4	43
122	Gadoxetate-enhanced abbreviated MRI is highly accurate for hepatocellular carcinoma screening. European Radiology, 2020, 30, 6003-6013.	4.5	43
123	Cardiac Steady-State Free Precession CINE Magnetic Resonance Imaging at 3.0 Tesla. Investigative Radiology, 2006, 41, 141-147.	6.2	42
124	Iterative Decomposition of Water and Fat with Echo Asymmetry and Least-Squares Estimation (IDEAL) Fast Spin-Echo Imaging of the Ankle: Initial Clinical Experience. American Journal of Roentgenology, 2006, 187, 1442-1447.	2.2	42
125	Improved least squares MR image reconstruction using estimates of <i>kâ€</i> Space data consistency. Magnetic Resonance in Medicine, 2012, 67, 1600-1608.	3.0	42
126	Variations in T2* and fat content of murine brown and white adipose tissues by chemical-shift MRI. Magnetic Resonance Imaging, 2012, 30, 323-329.	1.8	42

#	Article	IF	CITATIONS
127	Emerging quantitative magnetic resonance imaging biomarkers of hepatic steatosis. Hepatology, 2013, 58, 1877-1880.	7.3	42
128	Cytochrome P450 1B1: An unexpected modulator of liver fatty acid homeostasis. Archives of Biochemistry and Biophysics, 2015, 571, 21-39.	3.0	42
129	High-Resolution 3D Cartilage Imaging with IDEAL–SPGR at 3 T. American Journal of Roentgenology, 2007, 189, 1510-1515.	2.2	41
130	Validation of MRI biomarkers of hepatic steatosis in the presence of iron overload in the ob/ob mouse. Journal of Magnetic Resonance Imaging, 2012, 35, 844-851.	3.4	41
131	Adipose tissue MRI for quantitative measurement of central obesity. Journal of Magnetic Resonance Imaging, 2013, 37, 707-716.	3.4	41
132	Longitudinal Monitoring of Hepatic Blood Flow before and after TIPS by Using 4D-Flow MR Imaging. Radiology, 2016, 281, 574-582.	7.3	41
133	Liver fat quantification: where do we stand?. Abdominal Radiology, 2020, 45, 3386-3399.	2.1	41
134	R2* estimation using "inâ€phase―echoes in the presence of fat: The effects of complex spectrum of fat. Journal of Magnetic Resonance Imaging, 2013, 37, 717-726.	3.4	40
135	Consensus report from the 6th International forum for liver MRI using gadoxetic acid. Journal of Magnetic Resonance Imaging, 2014, 40, 516-529.	3.4	40
136	Quantitative cardiac perfusion: a noninvasive spin-labeling method that exploits coronary vessel geometry Radiology, 1996, 200, 177-184.	7.3	39
137	Single acquisition water-fat separation: Feasibility study for dynamic imaging. Magnetic Resonance in Medicine, 2006, 55, 413-422.	3.0	39
138	Fat confounds the observed apparent diffusion coefficient in patients with hepatic steatosis. Magnetic Resonance in Medicine, 2013, 69, 545-552.	3.0	39
139	Emerging Applications of Abdominal 4D Flow MRI. American Journal of Roentgenology, 2016, 207, 58-66.	2.2	39
140	Diagnostic Accuracy of MRI Versus CT for the Evaluation of Acute Appendicitis in Children and Young Adults. American Journal of Roentgenology, 2017, 209, 911-919.	2.2	39
141	Quantification of liver fat in the presence of iron overload. Journal of Magnetic Resonance Imaging, 2017, 45, 428-439.	3.4	39
142	Linearity and Bias of Proton Density Fat Fraction as a Quantitative Imaging Biomarker: A Multicenter, Multiplatform, Multivendor Phantom Study. Radiology, 2021, 298, 640-651.	7.3	39
143	Improved delayed enhanced myocardial imaging with T ₂ â€Prep inversion recovery magnetization preparation. Journal of Magnetic Resonance Imaging, 2008, 28, 1280-1286.	3.4	38
144	T1 bias in chemical shiftâ€encoded liver fatâ€fraction: Role of the flip angle. Journal of Magnetic Resonance Imaging, 2014, 40, 875-883.	3.4	38

#	Article	IF	CITATIONS
145	Four-dimensional Flow MRI as a Marker for Risk Stratification of Gastroesophageal Varices in Patients with Liver Cirrhosis. Radiology, 2019, 290, 101-107.	7.3	38
146	Tag contrast in breath-hold CINE cardiac MRI. Magnetic Resonance in Medicine, 1994, 31, 521-525.	3.0	37
147	Magnetic susceptibility as a <i>B</i> ₀ field strength independent MRI biomarker of liver iron overload. Magnetic Resonance in Medicine, 2013, 70, 648-656.	3.0	36
148	Prospective Comparison of the Diagnostic Accuracy of MR Imaging versus CT for Acute Appendicitis. Radiology, 2018, 288, 467-475.	7.3	36
149	IDEAL-IQ in an oncologic population: meeting the challenge of concomitant liver fat and liver iron. Cancer Imaging, 2018, 18, 51.	2.8	36
150	Cartilage morphology at 3.0T: Assessment of threeâ€ d imensional magnetic resonance imaging techniques. Journal of Magnetic Resonance Imaging, 2010, 32, 173-183.	3.4	35
151	Load-dependent variations in knee kinematics measured with dynamic MRI. Journal of Biomechanics, 2013, 46, 2045-2052.	2.1	35
152	Constraining the initial phase in water–fat separation. Magnetic Resonance Imaging, 2011, 29, 216-221.	1.8	34
153	Gadoxetic acid–enhanced T1â€weighted MR cholangiography in primary sclerosing cholangitis. Journal of Magnetic Resonance Imaging, 2012, 36, 632-640.	3.4	34
154	Longitudinal Changes in Liver Fat Content in Asymptomatic Adults: Hepatic Attenuation on Unenhanced CT as an Imaging Biomarker for Steatosis. American Journal of Roentgenology, 2015, 205, 1167-1172.	2.2	34
155	Systematic review and metaâ€analysis of the accuracy of MRI to diagnose appendicitis in the general population. Journal of Magnetic Resonance Imaging, 2016, 43, 1346-1354.	3.4	34
156	Contrast enhanced pulmonary magnetic resonance angiography for pulmonary embolism: Building a successful program. European Journal of Radiology, 2016, 85, 553-563.	2.6	32
157	Multiecho IDEAL Gradient-Echo Water-Fat Separation for Rapid Assessment of Cartilage Volume at 1.5 T: Initial Experience. Radiology, 2009, 252, 561-567.	7.3	31
158	Increased volume of coverage for abdominal contrastâ€enhanced MR angiography with twoâ€dimensional autocalibrating parallel imaging: Initial experience at 3.0 Tesla. Journal of Magnetic Resonance Imaging, 2009, 30, 1093-1100.	3.4	30
159	Predicting Hepatic Steatosis in a Racially and Ethnically Diverse Cohort of Adolescent Girls. Journal of Pediatrics, 2014, 165, 319-325.e1.	1.8	30
160	Highâ€spatial and highâ€ŧemporal resolution dynamic contrastâ€enhanced perfusion imaging of the liver with timeâ€resolved threeâ€dimensional radial MRI. Magnetic Resonance in Medicine, 2014, 71, 934-941.	3.0	29
161	The Impact of the COVID-19 Pandemic on the Radiology Research Enterprise: Radiology Scientific Expert Panel. Radiology, 2020, 296, E134-E140.	7.3	29
162	A novel object-independent ?balanced? reference scan for echo-planar imaging. Journal of Magnetic Resonance Imaging, 1999, 9, 847-852.	3.4	28

#	Article	IF	CITATIONS
163	Improved fat suppression using multipeak reconstruction for IDEAL chemical shift fatâ€water separation: Application with fast spin echo imaging. Journal of Magnetic Resonance Imaging, 2009, 29, 436-442.	3.4	28
164	T ₂ â€weighted 3D fast spin echo imaging with water–fat separation in a single acquisition. Journal of Magnetic Resonance Imaging, 2010, 32, 745-751.	3.4	28
165	Effect of temporal resolution on 4D flow MRI in the portal circulation. Journal of Magnetic Resonance Imaging, 2014, 39, 819-826.	3.4	28
166	Pulmonary Embolism Detection with Three-dimensional Ultrashort Echo Time MR Imaging: Experimental Study in Canines. Radiology, 2016, 278, 413-421.	7.3	28
167	Non-contrast-enhanced MRA of renal artery stenosis: validation against DSA in a porcine model. European Radiology, 2016, 26, 547-555.	4.5	28
168	Balanced SSFP imaging of the musculoskeletal system. Journal of Magnetic Resonance Imaging, 2007, 25, 270-278.	3.4	27
169	Simultaneous estimation of tongue volume and fat fraction using IDEALâ€FSE. Journal of Magnetic Resonance Imaging, 2008, 28, 504-508.	3.4	27
170	Improving chemical shift encoded water–fat separation using objectâ€based information of the magnetic field inhomogeneity. Magnetic Resonance in Medicine, 2015, 73, 597-604.	3.0	27
171	MRI proton density fat fraction is robust across the biologically plausible range of triglyceride spectra in adults with nonalcoholic steatohepatitis. Journal of Magnetic Resonance Imaging, 2018, 47, 995-1002.	3.4	27
172	Steady-State Free Precession MR Imaging: Improved Myocardial Tag Persistence and Signal-to-Noise Ratio for Analysis of Myocardial Motion. Radiology, 2004, 230, 852-861.	7.3	26
173	Gadolinium Deposition in the Brain: Do We Know Enough to Change Practice?. Radiology, 2016, 279, 323-326.	7.3	26
174	Thermogenic profiling using magnetic resonance imaging of dermal and other adipose tissues. JCI Insight, 2016, 1, e87146.	5.0	26
175	Controversies in Protocol Selection in the Imaging of Articular Cartilage. Seminars in Musculoskeletal Radiology, 2005, 9, 161-172.	0.7	24
176	Effects of injection rate and dose on image quality in time-resolved magnetic resonance angiography (MRA) by using 1.0M contrast agents. European Radiology, 2007, 17, 1394-1402.	4.5	24
177	<i>k</i> â€space waterâ€fat decomposition with T ₂ * estimation and multifrequency fat spectrum modeling for ultrashort echo time imaging. Journal of Magnetic Resonance Imaging, 2010, 31, 1027-1034.	3.4	24
178	Quantification of liver fat with respiratoryâ€gated quantitative chemical shift encoded MRI. Journal of Magnetic Resonance Imaging, 2015, 42, 1241-1248.	3.4	24
179	Surgical planning for living donor liver transplant using 4D flow MRI, computational fluid dynamics and in vitro experiments. Computer Methods in Biomechanics and Biomedical Engineering: Imaging and Visualization, 2018, 6, 545-555.	1.9	24
180	Simultaneous Noninvasive Determination of Regional Myocardial Perfusion and Oxygen Content in Rabbits: Toward Direct Measurement of Myocardial Oxygen Consumption at MR Imaging. Radiology, 1999, 212, 739-747.	7.3	23

#	Article	IF	CITATIONS
181	Cartilage imaging at 3.0T with gradient refocused acquisition in the steadyâ€state (GRASS) and IDEAL fatâ€water separation. Journal of Magnetic Resonance Imaging, 2008, 28, 167-174.	3.4	23
182	Robust multipoint waterâ€fat separation using fat likelihood analysis. Magnetic Resonance in Medicine, 2012, 67, 1065-1076.	3.0	23
183	Optimal Timing and Diagnostic Adequacy of Hepatocyte Phase Imaging with Gadoxetate-Enhanced Liver MRI. Academic Radiology, 2014, 21, 726-732.	2.5	23
184	Reproducibility of Cerebrospinal Venous Blood Flow and Vessel Anatomy with the Use of Phase Contrast-Vastly Undersampled Isotropic Projection Reconstruction and Contrast-Enhanced MRA. American Journal of Neuroradiology, 2014, 35, 999-1006.	2.4	23
185	Perfusion of the placenta assessed using arterial spin labeling and ferumoxytol dynamic contrast enhanced magnetic resonance imaging in the rhesus macaque. Magnetic Resonance in Medicine, 2019, 81, 1964-1978.	3.0	23
186	Contrast-enhanced pulmonary MRA for the primary diagnosis of pulmonary embolism: current state of the art and future directions. British Journal of Radiology, 2017, 90, 20160901.	2.2	22
187	The effects of concomitant gradients on chemical shift encoded MRI. Magnetic Resonance in Medicine, 2017, 78, 730-738.	3.0	22
188	Monitoring Fatty Liver Disease with MRI Following Bariatric Surgery: A Prospective, Dual-Center Study. Radiology, 2019, 290, 682-690.	7.3	22
189	Comparison of radial 4D Flow-MRI with perivascular ultrasound to quantify blood flow in the abdomen and introduction of a porcine model of pre-hepatic portal hypertension. European Radiology, 2017, 27, 5316-5324.	4.5	21
190	Diagnostic Performance of MRI for Esophageal Carcinoma: A Systematic Review and Meta-Analysis. Radiology, 2021, 299, 583-594.	7.3	21
191	Techniques for high-speed cardiac magnetic resonance imaging in rats and rabbits. Magnetic Resonance in Medicine, 1997, 37, 124-130.	3.0	20
192	Flowâ€independent T ₂ â€prepared inversion recovery blackâ€blood MR imaging. Journal of Magnetic Resonance Imaging, 2010, 31, 248-254.	3.4	20
193	Optimization of regionâ€ofâ€interest sampling strategies for hepatic MRI proton density fat fraction quantification. Journal of Magnetic Resonance Imaging, 2018, 47, 988-994.	3.4	20
194	Complex confounder-corrected R2* mapping for liver iron quantification with MRI. European Radiology, 2021, 31, 264-275.	4.5	20
195	Single breathhold cardiac CINE imaging with multiâ€echo threeâ€dimensional hybrid radial SSFP acquisition. Journal of Magnetic Resonance Imaging, 2010, 32, 434-440.	3.4	19
196	64â€MULTIDETECTOR COMPUTED TOMOGRAPHIC ANGIOGRAPHY OF THE CANINE CORONARY ARTERIES. Veterinary Radiology and Ultrasound, 2011, 52, 507-515.	0.9	19
197	Interleaved variable density sampling with a constrained parallel imaging reconstruction for dynamic contrastâ€enhanced MR angiography. Magnetic Resonance in Medicine, 2011, 66, 428-436.	3.0	19
198	Characterizing the limits of MRI near metallic prostheses. Magnetic Resonance in Medicine, 2015, 74, 1564-1573.	3.0	19

#	Article	IF	CITATIONS
199	Accuracy of PDFF estimation by magnitudeâ€based and complexâ€based MRI in children with MR spectroscopy as a reference. Journal of Magnetic Resonance Imaging, 2017, 46, 1641-1647.	3.4	19
200	High specificity targeting and detection of human neuroblastoma using multifunctional anti-GD2 iron-oxide nanoparticles. Nanomedicine, 2015, 10, 2973-2988.	3.3	18
201	Improved timeâ€ofâ€flight magnetic resonance angiography with IDEAL waterâ€fat separation. Journal of Magnetic Resonance Imaging, 2009, 29, 1367-1374.	3.4	17
202	Contrast-Enhanced Abdominal MRI for Suspected Appendicitis: How We Do It. American Journal of Roentgenology, 2016, 207, 49-57.	2.2	17
203	Feasibility of high spatiotemporal resolution for an abbreviated 3 <scp>D</scp> radial breast <scp>MRI</scp> protocol. Magnetic Resonance in Medicine, 2018, 80, 1452-1466.	3.0	17
204	Noise properties of proton density fat fraction estimated using chemical shift–encoded MRI. Magnetic Resonance in Medicine, 2018, 80, 685-695.	3.0	17
205	B ₀ and B ₁ inhomogeneities in the liver at 1.5 T and 3.0 T. Magnetic Resonance in Medicine, 2021, 85, 2212-2220.	3.0	17
206	Measurement of Signal-to-Noise Ratio and Parallel Imaging. , 2007, , 49-61.		17
207	Ultrafast Pulse Sequence Techniques for Cardiac Magnetic Resonance Imaging. Topics in Magnetic Resonance Imaging, 2000, 11, 312-330.	1.2	16
208	Advanced MR imaging of the shoulder: dedicated cartilage techniques. Magnetic Resonance Imaging Clinics of North America, 2004, 12, 143-159.	1.1	16
209	Noise analysis for 3â€point chemical shiftâ€based waterâ€fat separation with spectral modeling of fat. Journal of Magnetic Resonance Imaging, 2010, 32, 493-500.	3.4	16
210	Reduction of image noise in low tube current dynamic CT myocardial perfusion imaging using HYPR processing: A timeâ€attenuation curve analysis. Medical Physics, 2013, 40, 011904.	3.0	16
211	MRI for acute chest pain: Current state of the Art. Journal of Magnetic Resonance Imaging, 2013, 37, 1290-1300.	3.4	16
212	Pulmonary MRA: Differentiation of pulmonary embolism from truncation artefact. European Radiology, 2014, 24, 1942-1949.	4.5	16
213	Effect of hepatocyte-specific gadolinium-based contrast agents on hepatic fat-fraction and R2âŽ. Magnetic Resonance Imaging, 2015, 33, 43-50.	1.8	16
214	Validation of a motionâ€robust 2D sequential technique for quantification of hepatic proton density fat fraction during free breathing. Journal of Magnetic Resonance Imaging, 2018, 48, 1578-1585.	3.4	16
215	Pilot study on longitudinal change in pancreatic proton density fat fraction during a weightâ€loss surgery program in adults with obesity. Journal of Magnetic Resonance Imaging, 2019, 50, 1092-1102.	3.4	16
216	Sensitivity of quantitative relaxometry and susceptibility mapping to microscopic iron distribution. Magnetic Resonance in Medicine, 2020, 83, 673-680.	3.0	16

#	Article	IF	CITATIONS
217	Accuracy of common proton density fat fraction thresholds for magnitude- and complex-based chemical shift-encoded MRI for assessing hepatic steatosis in patients with obesity. Abdominal Radiology, 2020, 45, 661-671.	2.1	16
218	Successful Computed Tomography Angiogram Through Tibial Intraosseous Access: A Case Report. Journal of Emergency Medicine, 2013, 45, 182-185.	0.7	15
219	Highâ€resolution 3D radial bSSFP with IDEAL. Magnetic Resonance in Medicine, 2014, 71, 95-104.	3.0	15
220	Clinical outcomes after magnetic resonance angiography (MRA) versus computed tomographic angiography (CTA) for pulmonary embolism evaluation. Emergency Radiology, 2018, 25, 469-477.	1.8	15
221	A New Intercostal Artery Management Strategy for Thoracoabdominal Aortic Aneurysm Repair. Journal of Surgical Research, 2009, 154, 99-104.	1.6	14
222	Cardiac MRI evaluation of nonischemic cardiomyopathies. Journal of Magnetic Resonance Imaging, 2010, 31, 518-530.	3.4	14
223	Trends in the Use of Medical Imaging to Diagnose Appendicitis at an Academic Medical Center. Journal of the American College of Radiology, 2016, 13, 1050-1056.	1.8	14
224	Incidence of actionable findings on contrast enhanced magnetic resonance angiography ordered for pulmonary embolism evaluation. European Journal of Radiology, 2016, 85, 1383-1389.	2.6	14
225	MRI liver fat quantification in an oncologic population: the added value of complex chemical shift-encoded MRI. Clinical Imaging, 2018, 52, 193-199.	1.5	14
226	Comparison of gadoliniumâ€enhanced and ferumoxytolâ€enhanced conventional and UTEâ€MRA for the depiction of the pulmonary vasculature. Magnetic Resonance in Medicine, 2019, 82, 1660-1670.	3.0	14
227	PULMONARY ANGIOGRAPHY WITH 64â€MULTIDETECTORâ€ROW COMPUTED TOMOGRAPHY IN NORMAL DOGS Veterinary Radiology and Ultrasound, 2011, 52, 362-367.	[•] 0.9	13
228	Quantitative hepatic perfusion modeling using DCEâ€MRI with sequential breathholds. Journal of Magnetic Resonance Imaging, 2014, 39, 853-865.	3.4	13
229	Spectrally resolved fully phaseâ€encoded threeâ€dimensional fast spinâ€echo imaging. Magnetic Resonance in Medicine, 2014, 71, 681-690.	3.0	13
230	Intraindividual Crossover Comparison of Gadoxetic Acid Dose for Liver MRI in Normal Volunteers. Magnetic Resonance in Medical Sciences, 2016, 15, 60-72.	2.0	13
231	An acetoneâ€based phantom for quantitative diffusion MRI. Journal of Magnetic Resonance Imaging, 2017, 46, 1683-1692.	3.4	13
232	Deep Brain Nuclei T1 Shortening after Gadobenate Dimeglumine in Children: Influence of Radiation and Chemotherapy. American Journal of Neuroradiology, 2018, 39, 24-30.	2.4	13
233	Clinical Implementation of a Focused MRI Protocol for Hepatic Fat and Iron Quantification. American Journal of Roentgenology, 2019, 213, 90-95.	2.2	13
234	Quantitative ferumoxytol-enhanced MRI in pregnancy: A feasibility study in the nonhuman primate. Magnetic Resonance Imaging, 2020, 65, 100-108.	1.8	13

#	Article	IF	CITATIONS
235	Pharmacokinetics of Ferumoxytol in the Abdomen and Pelvis: A Dosing Study with 1.5- and 3.0-T MRI Relaxometry. Radiology, 2020, 294, 108-116.	7.3	13
236	Design of kâ€space channel combination kernels and integration with parallel imaging. Magnetic Resonance in Medicine, 2014, 71, 2139-2154.	3.0	12
237	Added value of gadoxetic acid-enhanced T1-weighted magnetic resonance cholangiography for the diagnosis of post-transplant biliary complications. European Radiology, 2017, 27, 4415-4425.	4.5	12
238	Recommendations for Imaging Patients With Cardiac Implantable Electronic Devices (<scp>CIEDs</scp>). Journal of Magnetic Resonance Imaging, 2021, 53, 1311-1317.	3.4	12
239	Waterâ€silicone separated volumetric MR acquisition for rapid assessment of breast implants. Journal of Magnetic Resonance Imaging, 2012, 35, 1216-1221.	3.4	11
240	Clinical Implications of Non–Contrast-Enhanced Computed Tomography for Follow-Up After Endovascular Abdominal Aortic Aneurysm Repair. Annals of Vascular Surgery, 2013, 27, 1042-1048.	0.9	11
241	Ethnic differences in the effects of hepatic fat deposition on insulin resistance in nonobese middle school girls. Obesity, 2014, 22, 243-248.	3.0	11
242	Accelerating sequences in the presence of metal by exploiting the spatial distribution of offâ€resonance. Magnetic Resonance in Medicine, 2014, 72, 1658-1667.	3.0	11
243	High SNR Acquisitions Improve the Repeatability of Liver Fat Quantification Using Confounder-corrected Chemical Shift-encoded MR Imaging. Magnetic Resonance in Medical Sciences, 2017, 16, 332-339.	2.0	11
244	Interâ€method reproducibility of biexponential <scp>R</scp> ₂ MR relaxometry for estimation of liver iron concentration. Magnetic Resonance in Medicine, 2018, 80, 2691-2701.	3.0	11
245	Hepatic steatosis and reduction in steatosis following bariatric weight loss surgery differs between segments and lobes. European Radiology, 2019, 29, 2474-2480.	4.5	11
246	Diurnal Variation of Proton Density Fat Fraction in the Liver Using Quantitative Chemical Shift Encoded MRI. Journal of Magnetic Resonance Imaging, 2020, 51, 407-414.	3.4	11
247	Temperatureâ€corrected proton density fat fraction estimation using chemical shiftâ€encoded MRI in phantoms. Magnetic Resonance in Medicine, 2021, 86, 69-81.	3.0	11
248	Clinical Applications of 4D Flow MRI in the Portal Venous System. Magnetic Resonance in Medical Sciences, 2022, 21, 340-353.	2.0	11
249	MR system operator: Recommended minimum requirements for performing MRI in human subjects in a research setting. Journal of Magnetic Resonance Imaging, 2015, 41, 899-902.	3.4	10
250	Combined gadoxetic acid and gadofosveset enhanced liver MRI: A feasibility and parameter optimization study. Magnetic Resonance in Medicine, 2016, 75, 318-328.	3.0	10
251	Combined gadoxetic acid and gadofosveset enhanced liver MRI for detection and characterization of liver metastases. European Radiology, 2017, 27, 32-40.	4.5	10
252	Noncontrast Chest Computed Tomographic Imaging of Obesity and the Metabolic Syndrome. Journal of Thoracic Imaging, 2019, 34, 126-135.	1.5	10

#	Article	IF	CITATIONS
253	T ₁ â€corrected quantitative chemical shiftâ€encoded MRI. Magnetic Resonance in Medicine, 2020, 83, 2051-2063.	3.0	10
254	Phaseâ€based T ₂ mapping with gradient echo imaging. Magnetic Resonance in Medicine, 2020, 84, 609-619.	3.0	10
255	Design and evaluation of quantitative MRI phantoms to mimic the simultaneous presence of fat, iron, and fibrosis in the liver. Magnetic Resonance in Medicine, 2021, 85, 734-747.	3.0	10
256	Limits of Fat Quantification in the Presence of Iron Overload. Journal of Magnetic Resonance Imaging, 2021, 54, 1166-1174.	3.4	10
257	Multisite multivendor validation of a quantitative MRI and CT compatible fat phantom. Medical Physics, 2021, 48, 4375-4386.	3.0	10
258	Abdominal applications of quantitative 4D flow MRI. Abdominal Radiology, 2022, 47, 3229-3250.	2.1	10
259	Non-Contrast Enhanced 3D SSFP MRA of the Renal Allograft Vasculature: A Comparison Between Radial Linear Combination and Cartesian Inflow-Weighted Acquisitions. Magnetic Resonance Imaging, 2014, 32, 190-195.	1.8	9
260	In Nonobese Girls, Waist Circumference as a Predictor of Insulin Resistance Is Comparable to MRI Fat Measures and Superior to BMI. Hormone Research in Paediatrics, 2015, 84, 258-265.	1.8	9
261	Mathematical optimization of contrast concentration for t ₁ â€weighted spoiled gradient echo imaging. Magnetic Resonance in Medicine, 2016, 75, 1556-1564.	3.0	9
262	Fully phaseâ€encoded MRI near metallic implants using ultrashort echo times and broadband excitation. Magnetic Resonance in Medicine, 2018, 79, 2156-2163.	3.0	9
263	Assessment of a highâ€6NR chemicalâ€shiftâ€encoded MRI with complex reconstruction for proton density fat fraction (PDFF) estimation overall and in the lowâ€fat range. Journal of Magnetic Resonance Imaging, 2019, 49, 229-238.	3.4	9
264	Use of chemical shift encoded magnetic resonance imaging (CSE-MRI) for high resolution fat-suppressed imaging of the brachial and lumbosacral plexuses. European Journal of Radiology, 2016, 85, 1199-1207.	2.6	8
265	MRI of the Nontraumatic Acute Abdomen. Gastroenterology Clinics of North America, 2018, 47, 667-690.	2.2	8
266	Evaluation of a motionâ€robust 2D chemical shiftâ€encoded technique for R2* and field map quantification in ferumoxytolâ€enhanced MRI of the placenta in pregnant rhesus macaques. Journal of Magnetic Resonance Imaging, 2020, 51, 580-592.	3.4	8
267	No Cases of Nephrogenic Systemic Fibrosis after Administration of Gadoxetic Acid. Radiology, 2020, 297, 556-562.	7.3	8
268	A Phase 1 Dose Escalation Study of Neoadjuvant SBRT Plus Elective Nodal Radiation with Concurrent Capecitabine for Resectable Pancreatic Cancer. International Journal of Radiation Oncology Biology Physics, 2021, 109, 458-463.	0.8	8
269	High temporal resolution cardiac cone-beam CT using a slowly rotating C-arm gantry. Proceedings of SPIE, 2009, , .	0.8	7
270	Improved fat water separation with water selective inversion pulse for inversion recovery imaging in cardiac MRI. Journal of Magnetic Resonance Imaging, 2013, 37, 484-490.	3.4	7

#	Article	IF	CITATIONS
271	Combined dynamic contrast-enhanced liver MRI and MRA using interleaved variable density sampling. Magnetic Resonance in Medicine, 2015, 73, 973-983.	3.0	7
272	On confirmation bias in imaging research. Journal of Magnetic Resonance Imaging, 2015, 41, 1163-1164.	3.4	7
273	Magnetic Resonance Angiography of the Upper Extremity. Magnetic Resonance Imaging Clinics of North America, 2015, 23, 479-493.	1.1	7
274	Externally calibrated parallel imaging for 3D multispectral imaging near metallic implants using broadband ultrashort echo time imaging. Magnetic Resonance in Medicine, 2017, 77, 2303-2309.	3.0	7
275	Comparison of ferumoxytolâ€based cerebral blood volume estimates using quantitative R ₁ and relaxometry. Magnetic Resonance in Medicine, 2018, 79, 3072-3081.	3.0	7
276	Vascular input function correction of inflow enhancement for improved pharmacokinetic modeling of liver <scp>DCE</scp> â€ <scp>MRI</scp> . Magnetic Resonance in Medicine, 2018, 79, 3093-3102.	3.0	7
277	Characterizing a short T ₂ * signal component in the liver using ultrashort TE chemical shiftâ€encoded MRI at 1.5T and 3.0T. Magnetic Resonance in Medicine, 2019, 82, 2032-2045.	3.0	7
278	Measurement of spleen fat on MRI-proton density fat fraction arises from reconstruction of noise. Abdominal Radiology, 2019, 44, 3295-3303.	2.1	7
279	Relaxivityâ€iron calibration in hepatic iron overload: Reproducibility and extension of a Monte Carlo model. NMR in Biomedicine, 2021, 34, e4604.	2.8	7
280	Single-shot, variable flip-angle slice-selective excitation with four gradient-modulated adiabatic half-passage segments. Magnetic Resonance in Medicine, 1998, 40, 334-340.	3.0	6
281	Temporally Targeted Imaging Method Applied to ECC-Gated Computed Tomography. Academic Radiology, 2008, 15, 93-106.	2.5	6
282	Noise considerations of three-point water-fat separation imaging methods. Medical Physics, 2008, 35, 3597-3606.	3.0	6
283	Navigator flip angle optimization for freeâ€breathing T1â€weighted hepatobiliary phase imaging with gadoxetic acid. Journal of Magnetic Resonance Imaging, 2014, 40, 1129-1136.	3.4	6
284	Wholeâ€heart chemical shift encoded water–fat MRI. Magnetic Resonance in Medicine, 2014, 72, 718-725.	3.0	6
285	Flow-induced signal misallocation artifacts in two-point fat-water chemical shift MRI. Magnetic Resonance in Medicine, 2015, 73, 1926-1931.	3.0	6
286	Accelerating fully phaseâ€encoded MRI near metal using multiband radiofrequency excitation. Magnetic Resonance in Medicine, 2017, 77, 1223-1230.	3.0	6
287	Crossover comparison of ferumoxytol and gadobenate dimeglumine for abdominal MRâ€angiography at 3.0 tesla: Effects of contrast bolus length and flip angle. Journal of Magnetic Resonance Imaging, 2017, 45, 1617-1626.	3.4	6
288	Magnetic resonance elastography biomarkers for detection of histologic alterations in nonalcoholic fatty liver disease in the absence of fibrosis. European Radiology, 2021, 31, 8408-8419.	4.5	6

#	Article	IF	CITATIONS
289	Spectroscopyâ€based multiâ€parametric quantification in subjects with liver iron overload at 1.5T and 3T. Magnetic Resonance in Medicine, 2022, 87, 597-613.	3.0	6
290	Emergence of 3D MR Elastography–based Quantitative Markers for Diffuse Liver Disease. Radiology, 2021, 301, 163-165.	7.3	6
291	ECG-gated HYPR reconstruction for undersampled CT myocardial perfusion imaging. , 2007, , .		6
292	Proton density water fraction as a reproducible MRâ€based measurement of breast density. Magnetic Resonance in Medicine, 2022, 87, 1742-1757.	3.0	6
293	Characterization of mesenteric and portal hemodynamics using 4D flow MRI: the effects of meals and diurnal variation. Abdominal Radiology, 2022, 47, 2106-2114.	2.1	6
294	Preface. Magnetic Resonance Imaging Clinics of North America, 2009, 17, xi-xii.	1.1	5
295	How to write an original radiological research manuscript. European Radiology, 2017, 27, 4455-4460.	4.5	5
296	Chelated or dechelated gadolinium deposition – Authors' reply. Lancet Neurology, The, 2017, 16, 955-956.	10.2	5
297	Thrombus-mimicking artifacts in two-point Dixon MRI: Prevalence, appearance, and severity. Journal of Magnetic Resonance Imaging, 2017, 45, 229-236.	3.4	5
298	Impact of ferumoxytol magnetic resonance imaging on the rhesus macaque maternal–fetal interfaceâ€. Biology of Reproduction, 2020, 102, 434-444.	2.7	5
299	Motionâ€robust, highâ€5NR liver fat quantification using a 2D sequential acquisition with a variable flip angle approach. Magnetic Resonance in Medicine, 2020, 84, 2004-2017.	3.0	5
300	Accuracies of Chemical Shift In/Opposed Phase and Chemical Shift Encoded Magnetic Resonance Imaging to Detect Intratumoral Fat in Hepatocellular Carcinoma. Journal of Magnetic Resonance Imaging, 2021, 53, 1791-1802.	3.4	5
301	Emerging quantitative MRI biomarkers of diffuse liver disease. Clinical Liver Disease, 2014, 4, 129-132.	2.1	4
302	Prospective evaluation of MRI compared with CT for the etiology of abdominal pain in emergency department patients with concern for appendicitis. Journal of Magnetic Resonance Imaging, 2019, 50, 1651-1658.	3.4	4
303	Magnetic resonance imaging versus computed tomography and ultrasound for the diagnosis of female pelvic pathology. Emergency Radiology, 2021, 28, 789-796.	1.8	4
304	Reproducibility of liver R2* quantification for liver iron quantification from cardiac R2* acquisitions. Abdominal Radiology, 2021, 46, 4200-4209.	2.1	4
305	Magnetic Resonance Imaging as an Alternative to <scp>Contrastâ€Enhanced</scp> Computed Tomography to Mitigate Iodinated Contrast Shortages in the United States: Recommendations From the International Society for Magnetic Resonance in Medicine. Journal of Magnetic Resonance Imaging, 2022. 56. 655-656.	3.4	4
306	Magnetic Resonance Imaging of Liver Fibrosis, Fat, and Iron. Radiologic Clinics of North America, 2022, 60, 705-716.	1.8	4

#	Article	IF	CITATIONS
307	Rapid comprehensive evaluation of luminography and hemodynamic function with 3d radially undersampled phase contrast imaging MRI. , 2009, 2009, 4057-60.		3
308	Frequency response of multipoint chemical shiftâ€based spectral decomposition. Journal of Magnetic Resonance Imaging, 2010, 32, 943-952.	3.4	3
309	Quantification of Liver Function with MRI: Is It Ready?. Radiology, 2019, 290, 134-135.	7.3	3
310	Dual contrast liver MRI: a pictorial illustration. Abdominal Radiology, 2021, 46, 4588-4600.	2.1	3
311	<scp>Magnetic Resonance</scp> Imaging During a Pandemic: Recommendations by the <scp>ISMRM</scp> Safety Committee. Journal of Magnetic Resonance Imaging, 2022, 55, 1322-1339.	3.4	3
312	Effect of temporal resolution on 4D flow MRI in the portal circulation. Journal of Magnetic Resonance Imaging, 2014, 39, spcone-spcone.	3.4	2
313	Gadolinium-based contrast agents: What does "single-dose―mean anymore?. Journal of Magnetic Resonance Imaging, 2014, 39, 1343-1345.	3.4	2
314	Application of direct virtual coil to dynamic contrastâ€enhanced MRI and MR angiography with dataâ€driven parallel imaging. Magnetic Resonance in Medicine, 2014, 71, 783-789.	3.0	2
315	Quantitative MRI Biomarkers of Diffuse Liver Disease. Advances in Clinical Radiology, 2019, 1, 55-69.	0.2	2
316	Combined gadoxetic acid and gadobenate dimeglumine enhanced liver MRI: a parameter optimization study. Abdominal Radiology, 2020, 45, 220-231.	2.1	2
317	Prospective comparison of longitudinal change in hepatic proton density fat fraction (PDFF) estimated by magnitude-based MRI (MRI-M) and complex-based MRI (MRI-C). European Radiology, 2020, 30, 5120-5129.	4.5	2
318	Freeâ€breathing liver fat and quantification using motionâ€corrected averaging based on a nonlocal means algorithm. Magnetic Resonance in Medicine, 2021, 85, 653-666.	3.0	2
319	Interobserver agreement for the direct and indirect signs of pulmonary embolism evaluated using contrast enhanced magnetic angiography. European Journal of Radiology Open, 2020, 7, 100256.	1.6	2
320	Addressing concomitant gradient phase errors in timeâ€interleaved chemical shiftâ€encoded MRI fat fraction and R 2 * mapping with a passâ€specific phase fitting method. Magnetic Resonance in Medicine, 2022, , .	3.0	2
321	"MR Physics for Clinicians―Series: Enhancement for the JMRI CME Program. Journal of Magnetic Resonance Imaging, 2012, 35, 997-997.	3.4	1
322	The evolving landscape of self-assessment continuing medical education (SA-CME). Journal of Magnetic Resonance Imaging, 2013, 38, 509-510.	3.4	1
323	New and Improved Imaging Modalities for NAFLD. Current Hepatology Reports, 2014, 13, 88-96.	0.9	1
324	CME update: Review articles and commentaries inJMRI. Journal of Magnetic Resonance Imaging, 2014, 40, 778-778.	3.4	1

#	Article	IF	CITATIONS
325	Primer on magnetic resonance imaging of the liver. Clinical Liver Disease, 2014, 4, 120-123.	2.1	1
326	Guidelines for documentation and consent for nonclinical, nonresearch MRI in human subjects. Journal of Magnetic Resonance Imaging, 2017, 45, 36-41.	3.4	1
327	MR visible localization device for radiographic-pathologic correlation of surgical specimens. Magnetic Resonance Imaging, 2017, 37, 159-163.	1.8	1
328	Feasibility and optimization of ultra-short echo time MRI for improved imaging of IVC-filters at 3.0ÂT. Abdominal Radiology, 2021, 46, 362-372.	2.1	1
329	Portosystemic Shunts: Should We Pay Closer Attention with Cross-Sectional Imaging?. Radiology, 2021, 299, 141-142.	7.3	1
330	Quantitative assessment of liver fat with magnetic resonance imaging and spectroscopy. , 2011, 34, 729.		1
331	Ferumoxytol-enhanced MR imaging for differentiating intrapancreatic splenules from other tumors. Abdominal Radiology, 2021, 46, 2003-2013.	2.1	1
332	Improved free-breathing liver fat and iron quantification using a 2D chemical shift–encoded MRI with flip angle modulation and motion-corrected averaging. European Radiology, 2022, 32, 5458-5467.	4.5	1
333	CE-MRA in the primary diagnosis of pulmonary embolism: Building a team to start a clinically relevant program. , 0, , 31-36.		1
334	Myosteatosis as a Shared Biomarker for Sarcopenia and Cachexia Using MRI and Ultrasound. Frontiers in Rehabilitation Sciences, 2022, 3, .	1.2	1
335	Whole chest MRA and velocimetry for congenital heart disease in less than 10 minutes with 3D radial phase contrast. Journal of Cardiovascular Magnetic Resonance, 2010, 12, .	3.3	Ο
336	Cardiac MR imaging. , 0, , 34-46.		0
337	In vivo validation of 4D flow MRI for assessing the hemodynamics of portal hypertension. Journal of Magnetic Resonance Imaging, 2013, 37, spcone-spcone.	3.4	Ο
338	Impaired regulation of portal venous flow in response to a meal challenge as quantified by 4D flow MRI. Journal of Magnetic Resonance Imaging, 2015, 42, spcone-spcone.	3.4	0
339	Quantification of liver proton-density fat fraction in 7.1T preclinical MR systems: Impact of the fitting technique. Journal of Magnetic Resonance Imaging, 2016, 44, 1425-1431.	3.4	Ο
340	Letter to the Editor: Intrapancreatic Accessory Spleen Masquerading as a Pancreatic Neuroendocrine Tumor. Journal of Gastrointestinal Surgery, 2019, 23, 1717-1718.	1.7	0
341	Effect of noise and estimator type on bias for analysis of liver proton density fat fraction. Magnetic Resonance Imaging, 2020, 74, 244-249.	1.8	Ο
342	Abdominal fellowship-trained versus generalist radiologist accuracy when interpreting MR and CT for the diagnosis of appendicitis. European Radiology, 2022, 32, 533-541.	4.5	0

#	Article	IF	CITATIONS
343	Editorial for "Effects of <scp>B₁</scp> Heterogeneity on Spin <scp>Echoâ€Based</scp> Liver Iron Estimates― Journal of Magnetic Resonance Imaging, 2022, 55, 1426-1427.	3.4	0
344	Simultaneous T 1 â€weighted and T 2 â€weighted 3D MRI using RF phaseâ€modulated gradient echo imaging. Magnetic Resonance in Medicine, 2021, 87, 1758.	3.0	0
345	Editorial for "Bias, Repeatability and Reproducibility of Liver <scp>T1</scp> Mapping With Variable Flip Anglesâ€, Journal of Magnetic Resonance Imaging, 2022, 56, 1053-1054.	3.4	0
346	Determining Biomarkers of Myosteatosis for Sarcopenia and Cachexia Using MRI and Ultrasound. FASEB Journal, 2022, 36, .	0.5	0